DOI: 10.1002/ejic.200700767

CO_2 Fixation and Activation by Cu^{II} Complexes of 5,5′′-Terpyridinophane Macrocycles

Begoña Verdejo,[a] Salvador Blasco,[a] Jorge González,[a] Enrique García-España,*[a] Pablo Gaviña,[b] Sergio Tatay,[b] Antonio Doménech,[c] María Teresa Doménech-Carbó,[d] Hermas R. Jiménez,[e] and Conxa Soriano[b]

Keywords: Macrocycles / N ligands / Copper / Carbon dioxide fixation / Electrochemistry

An aza-terpyridinophane receptor containing the polyamine 4,7,10,13-tetraazahexadecane-1,16-diamine linked through methylene groups to the 5,5′′ positions of a terpyridine unit has been prepared and characterized (L). The acid-base behaviour, Cu^{II} speciation and ability to form ternary complexes (Cu^{II}-L-carbonate) have been explored by potentiometric titrations in 0.15 M $NaClO_4$ and by UV/Vis and paramagnetic NMR spectroscopy. Comparisons are made with a previously reported terpyridinophane containing the polyamine 4,7,10-triazatridecane-1,13-diamine (L^1). For this latter receptor, reductive coupling between indigo and carbon dioxide at indigo-modified electrodes produces carboxylated derivatives via a solid-state reaction under electrochemical activation.

Introduction

CO_2 fixation and activation is a topic of paramount relevance in scientific research, which is why many researchers have devoted their efforts over the last few years to finding ways of reutilizing the current excess of atmospheric carbon dioxide for the production of chemicals of high industrial importance.[1,2]

Biological systems often offer scientists interesting hints about the way in which these challenging processes can be approached. In this sense, the enzyme *rubisco*, which is present in all photosynthetic systems participating in the first step of the Calvin cycle, shows the formation of a carbamate bond between atmospheric carbon dioxide and a lysine group in its active site in a process which is assisted by Mg^{II} or Mn^{II} ions as Lewis acids.[3] This elusive carbamate moiety is further stabilised by hydrogen bonding with other amino acid residues of the polypetide chain.

Following this idea, we have recently reported on the Cu^{II} and Zn^{II} complexes of a terpyridinophane-type receptor which is able to fix atmospheric CO_2 at neutral pH without the need for bubbling the gas into the solution (L^1 above).[4,5] L^1 is composed of a terpyridine unit that is connected at its 5,5′′ positions through methylene groups to the polyamine 4,7,10-triazatridecane-1,13-diamine. The terpyridine unit is able to block the metal ion at that side of the molecule while the polyamine bridge is flexible and basic enough to permit the metallo-assisted formation of the carbamate bond at neutral pH and its stabilisation by hydrogen bonding with protonated amino groups along the chain. These characteristics are clearly shown by the crystal structure of the complex $[Cu(HL^1\text{-carb})](ClO_4)_3{\cdot}2H_2O$.[4] We also observed that carbon dioxide fixation also occurs when Zn^{II} replaces Cu^{II}, thereby indicating that CO_2 fixation is independent of the metal ion used as long as its Lewis acid role is preserved.[5]

Here, we turn our attention to the polyamine bridge and explore whether the dimensionality and basic properties of L^1 are critical or whether other basic polyamines can perform the same job. To check this point we have substituted the polyamine bridge in L^1 by the hexaamine 4,7,10,13-tetraazahexadecane-1,16-diamine (L^2)[6] and have synthesized the new macrocycle L. We examine its complexing proper-

[a] Departament de Química Inorgànica, Institut de Ciència Molecular (ICMOL),Universitat de València, Edificio de Institutos de Paterna,
Apartado de Correos 22085, 46071 Valencia, Spain
Fax: +34-96-354-3274
E-mail: enrique.garcia-es@uv.es
[b] Departament de Química Orgànica, Institut de Ciència Molecular (ICMOL), Universitat de València, Edificio de Institutos de Paterna,
Apartado de Correos 22085, 46071 Valencia, Spain
[c] Departament de Química Analítica, Universitat de València, Dr. Moliner 50, 46100 Burjassot (Valencia), Spain
[d] Institut de Restauració del Patrimoni/Departament de Conservació i Restauració de Bens Culturals, Universitat Politècnica de València,
Camí de Vera 14, 46022, Valencia, Spain
[e] Departament de Química Inorgánica, Universitat de València, Dr. Moliner 50, 46100 Burjassot (Valencia), Spain

Supporting information for this article is available on the WWW under http://www.eurjic.org or from the author.

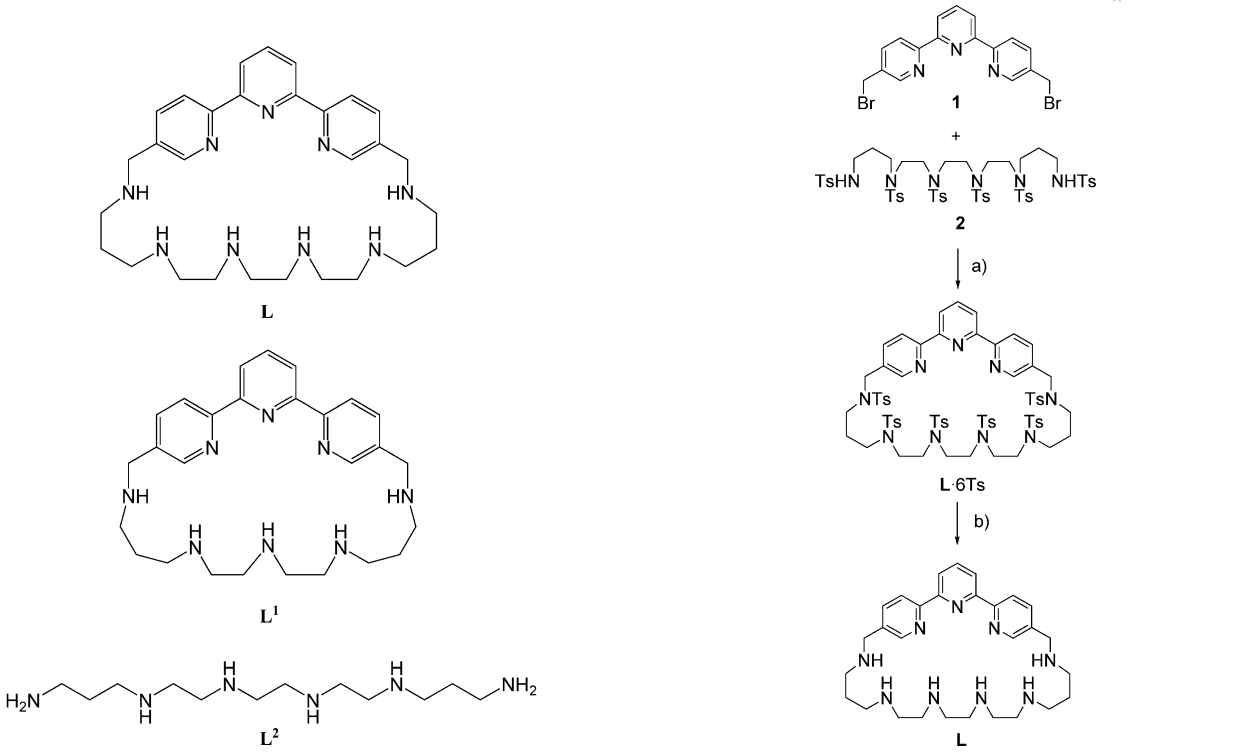

Scheme 1. a) K_2CO_3, CH_3CN, reflux (41%); b) HBr/HOAc, PhOH, reflux (97%).

ties towards Cu^{II} ions in aqueous solution and the ability to form ternary Cu^{II}:L/carbonate complexes (carbonate refers to the free anion or any of its protonated forms). Finally, in the last part of our contribution we discuss the possibility of using the receptor L^1 to catalyze the addition of CO_2 to the dye indigo, which represents a first outcome of this chemistry in CO_2 activation. Indigo [2-(1,3-dihydro-3-oxo-2*H*-indol-2-ylidene)-1,2-dihydro-3*H*-indol-3-one) is a quasi-planar molecule that has a slightly elongated central C=C bond and exhibits a well-defined solid-state electrochemistry that results in the oxidative formation of dehydroindigo and the reductive formation of leucoindigo.[7–9] Easy electrochemical interconversion between such indigo forms makes this system a promising candidate for monitoring electrochemically induced reactivity in solid phases.

Results and Discussion

Synthesis of L

The preparation of L followed a similar procedure to that previously reported for L^1 (see Scheme 1).[5] Thus, treatment of 5,5′′-bis(bromomethyl)terpyridine (**1**)[7] with the pertosylated enlarged open-chain polyamine **2**[6] in dry CH_3CN in the presence of K_2CO_3 gives pertosylated L in about 40% yield. Cleavage of the tosylamide groups by treatment with an HOAc/HBr mixture in the presence of a large excess of phenol yields compound L as its hydrobromide salt in 97% yield.

Acid–Base Behaviour

Table 1 lists the logarithms of the stepwise protonation constants of L, as calculated by pH-metric titration using the HYPERQUAD set of programs.[10] We also include the previously published constants for L^1, L^2 and those of the pyridinophane L^3 (see Scheme 2), which contains the same bridge but with pyridine instead of terpyridine as spacer, for comparison.[5,6,11]

Table 1. Logarithms of the protonation constants of the receptors L, L^1, L^2 and L^3 determined in 0.15 M $NaClO_4$ at 298.1 K.

Reaction[a]	L	L^1[b]	L^2[c]	L^3[d]
$L + H \leftrightarrows HL$	9.35(3)[e]	9.21(1)	10.84(1)	10.04(2)
$HL + H \leftrightarrows H_2L$	8.98(1)	8.17(3)	9.97(1)	9.43(2)
$H_2L + H \leftrightarrows H_3L$	7.63(1)	7.04(3)	8.99(1)	8.45(2)
$H_3L + H \leftrightarrows H_4L$	6.87(1)	5.74(4)	8.07(1)	7.53(2)
$H_4L + H \leftrightarrows H_5L$	5.81(1)	3.82(4)	5.91(2)	5.89(2)
$H_5L + H \leftrightarrows H_6L$	3.79(1)	3.27(4)	3.16(2)	2.83(2)
$H_6L + H \leftrightarrows H_7L$	2.58(2)	–	–	–
$\log\beta$[f]	45.01	37.25	46.94	44.18

[a] Charges omitted. [b] Values taken from ref.[5] [c] Values taken from ref.[6] [d] Values taken from ref.[11] [e] Values in parentheses are standard deviations in the last significant figure. [f] Global basicity constant ($\beta = \Pi K_{hjL}$).

It is interesting to note that the macrocycle L is less basic than the open-chain polyamine L^2 and the related pyridinophane L^3. This basicity reduction, which is particularly noticeable in the first four protonation steps and has already been observed for the related cyclophane L^1, can be ascribed to: i) the presence of primary nitrogens in L^2, which are more basic in water due to a more favourable solvation,

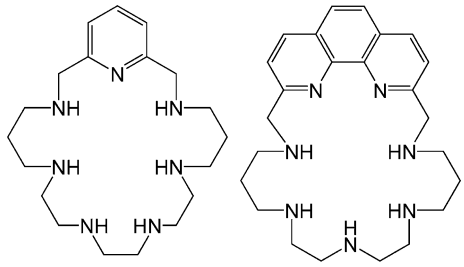

L^3 L^4

Scheme 2.

ii) the higher flexibility of the open-chain compound, which permits a more efficient separation of positive charges,[12] and iii) the electron-withdrawing characteristics of the terpyridine ring, which are better that of a single pyridine ring.

As is also the case for L^1, the number of protonation constants observed exceeds the number of amine groups in the chain by one; this extra protonation should occur on the pyridine nitrogens of the terpyridine moiety. To decide at what stage the terpyridine fragment is involved in protonation, we monitored the variation of the UV/Vis spectrum of L with pH (Figure 1). The spectrum of L at basic pH consists of two broad bands centred at 230 and 290 nm and remains essentially unchanged from pH 10.5 to pH 3.9. Below this pH, the band at 290 nm (ε = 19119 $M^{-1}cm^{-1}$) splits into two bands centred at 280 and 330 nm (ε = 14,414 and 12,515 $M^{-1}cm^{-1}$ respectively). It is well-known[13] that the initial band at 290 nm is the result of two π–π^* overlapped transitions with their dipolar moments oriented along the larger and shorter axes of the terpyridine unit. The latter transition is more sensitive to protonation and this is the band that appears bathochromically shifted at 330 nm when protonation of the terpyridine occurs. The pH value at which this splitting occurs suggests that protonation of the terpyridine occurs in the last protonation step.

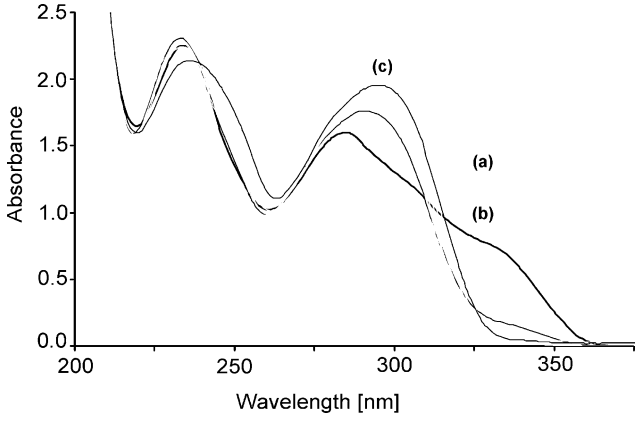

Figure 1. pH dependence of the absorption spectrum of L: (a) pH 2.51, (b) pH 3.12, (c) pH 3.89–10.56.

Cu^{II} Coordination

Tables 2, 3 and 4 collect the stability constants for Cu^{II} complexes formed by the new ligand L along with those previously reported for L^1, the open-chain polyamine L^2 and the pyridinophane L^3. The first aspect that deserves mentioning is that, as opposed to L^1, L^2 and L^3, L even forms trinuclear species which for a 3:1 M/L molar ratio are predominant in solution above pH 6, as can be seen in the distribution diagram plotted in Figure 2C.

As regards the formation of mononuclear species, the number of highly protonated species formed merits a mention (see Table 2). The protonation degree of 6 reached at low pH values in the mononuclear complexes ($[Cu(H_6L)]^{8+}$ species), which equals the number of amine groups present in the bridge, suggests that L, as is the case for L^1, is able to coordinate the metal ion through the terpyridine fragment even when the nitrogens of the polyamine chain are protonated. Molecular models indicate that the distances between the copper ion and any one of the protonated amino groups exceeds 5 Å, which means that Coulombic repulsions between them will not be significant. This is also supported by the values of the protonation constants of the complexes (entries 3–8 in Table 2), which compare favourably with the constants of the protonation steps of the free ligand with same overall charges [$CuL^{2+} + H^+ = CuHL^{3+}$, $\log K$ = 8.49(2) (entry 3 in Table 2) and $H_2L^{2+} + H^+ = H_3L^{3+}$, log K = 7.63(1), etc.].

The constant for the formation of the $[CuL]^{2+}$ complex, on the other hand, is lower than that previously reported for the $[CuL^3]^{2+}$ complex in which the nitrogen atoms of the polyamine chain participate in the binding of Cu^{II}.[13]

Table 2. Selected logarithms of the stability constants for the mononuclear copper complexes of the receptors L, L^1, L^2 and L^3 determined in 0.15 M $NaClO_4$ at 298.1 K.

Entry	Reaction[a]	L	L^{1}[c]	L^{2}[d]	L^{3}[e]
1	$M + L \leftrightarrows ML$	16.34(7)[b]	≈13.1	21.74(4)	19.29(3)
2	$M + L + 2H_2O \leftrightarrows ML(OH)_2 + 2H$	–3.8(1)	–	–	–
3	$ML + H \leftrightarrows MHL$	8.49(2)	≈9.7	10.06(3)	9.64(3)
4	$MHL + H \leftrightarrows MH_2L$	7.58(1)	7.38(1)	6.60(2)	6.71(2)
5	$MH_2L + H \leftrightarrows MH_3L$	6.58(1)	6.23(1)	3.48(2)	3.36(2)
6	$MH_3L + H \leftrightarrows MH_4L$	6.01(6)	5.46(1)	–	–
7	$MH_4L + H \leftrightarrows MH_5L$	5.11(6)	3.93(1)	–	–
8	$MH_5L + H \leftrightarrows MH_6L$	2.81(1)	–	–	–

[a] Charges omitted. [b] Values taken from ref.[5] [c] Values taken from ref.[6] [d] Values taken from ref.[11] [e] Values in parentheses are standard deviations in the last significant figure.

Table 3. Selected logarithms of the stability constants for the binuclear copper complexes of the receptors L, L^1, L^2 and L^3 determined in 0.15 M $NaClO_4$ at 298.1 K.

Entry	Reaction[a]	L	L^{1}[c]	L^{2}[d]	L^{3}[e]
1	$2M + L \leftrightarrows M_2L$	29.87(6)[b]	25.54(7)	–	30.21(2)
2	$M + ML \leftrightarrows M_2L$	13.53(7)	≈12.4	–	10.92(5)
3	$M_2L + H \leftrightarrows M_2HL$	6.56(7)	6.38(1)	–	4.63(3)
4	$M_2LH + H \leftrightarrows M_2H_2L$	6.01(7)	5.41(2)	–	–
5	$M_2LH_2 + H \leftrightarrows M_2H_3L$	4.70(9)	–	–	–
6	$2M + L + H_2O \leftrightarrows M_2L(OH) + H$	22.52(6)	18.78(8)	23.73(2)	20.14(2)
7	$2M + L + 2H_2O \leftrightarrows M_2L(OH)_2 + H$	13.93(7)	8.43(8)	–	–
8	$M_2L + H_2O \leftrightarrows M_2L(OH) + H$	–7.35(9)	–6.76(2)	–	–10.07(2)
9	$M_2L(OH) + 2H_2O \leftrightarrows M_2L(OH)_2 + H$	–8.59(7)	–10.35(1)	–	–

[a] Charges omitted. [b] Values taken from ref.[5] [c] Values taken from ref.[6] [d] Values taken from ref.[11] [e] Values in parentheses are standard deviations in the last significant figure.

Table 4. Selected logarithms of the stability constants for the trinuclear copper complexes of the receptor L determined in 0.15 M $NaClO_4$ at 298.1 K.

Entry	Reaction[a]	L
1	$3M + L + H_2O \leftrightarrows M_3L(OH) + H$	27.51(3)[b]
2	$3M + L + 2H_2O \leftrightarrows M_3L(OH)_2 + H$	20.48(7)
3	$3M + L + 3H_2O \leftrightarrows M_3L(OH)_3 + H$	14.02(2)

[a] Charges omitted. [b] Values in parentheses are standard deviations in the last significant figure.

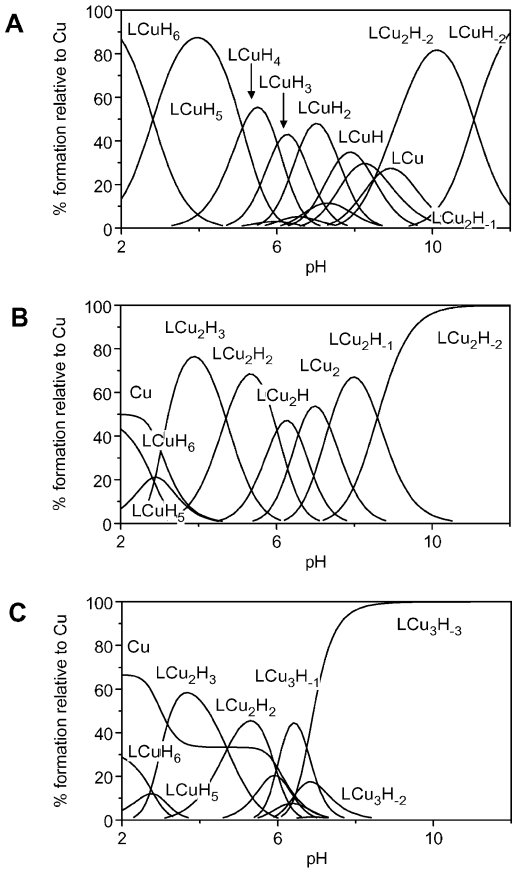

Figure 2. Distribution diagram for the system Cu^{II}-L: (A) molar ratio 1:1 $[Cu^{II}] = [L] = 10^{-3}$ M; (B) molar ratio 2:1 $[Cu^{II}] = 2 \times 10^{-3}$ M, $[L] = 10^{-3}$ M; (C) molar ratio 3:1 $[Cu^{II}] = 3 \times 10^{-3}$ M, $[L] = 10^{-3}$ M.

These data suggest that Cu^{II} is fixed at the terpyridine site and does not move to the polyamine site when raising the pH. This would again agree with the observed behaviour of L^1 and differs from a similar macrocycle that has the same polyamine chain as L^1 but a phenanthroline instead of a terpyridine spacer (L^4; Scheme 2).[14] The fixation of Cu^{II} at the terpyridine ring is also supported by the UV/Vis spectra (Figure 3). Thus, in the presence of an equimolar amount of Cu^{II} the spectra always show a two band pattern in the UV region similar to that observed when protonation of terpyridine occurs, thereby confirming that Cu^{II} binds at this side of the receptor and does not migrate to the polyamine bridge when raising the pH.

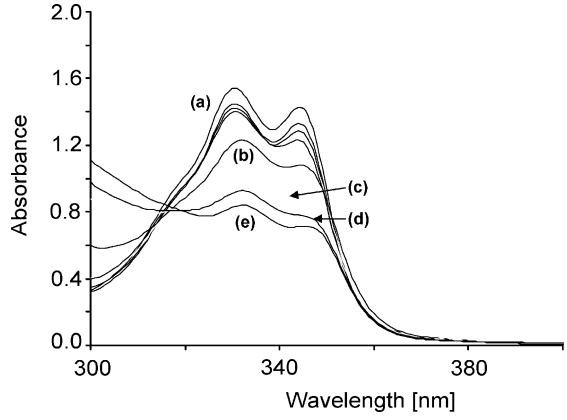

Figure 3. pH dependence of the absorption spectra of Cu^{II}/L in a 1:1 M:L molar ratio: (a) pH 2.30–6.52; (b) pH 7.17; (c) pH 8.35; (d) pH 9.07; (e) pH 10.33.

As seen from the distribution diagram in Figure 2B for a 2:1 Cu/L molar ratio the binuclear species $[Cu_2H_xL]^{(4+x)+}$ (x = 0–3) predominate in aqueous solution from pH 3 to 7. Above pH 7, however, the hydroxylated species $[Cu_2L(OH)]^{3+}$ and $[Cu_2L(OH)_2]^{2+}$ start to prevail. The presence of a triply protonated species indicates that three should be the minimum number of amine groups involved in the coordination; in this species one of the Cu^{II} will be fixed by the terpyridine nitrogen atoms while, taking into account the previously reported structure of $[Cu_2H_2L^1(CO_3)]_2(ClO_4)_8 \cdot 9H_2O$,[4] the other one will be most likely bound to the central nitrogens of the polyamine bridge (see Scheme 3A).

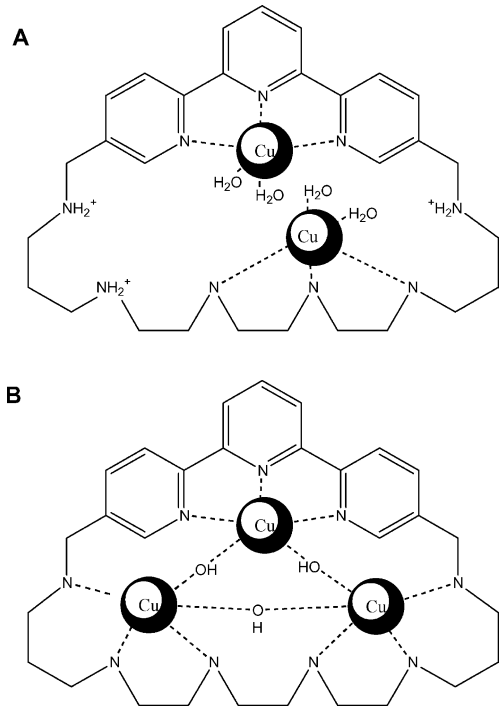

Scheme 3. Proposed structures for $[Cu_2(H_3L)]^{7+}$ (A) and $[Cu_3L(OH)_3]^{3+}$ (B).

The involvement of the terpyridine moiety in coordination to the metal ion is again confirmed by the 200–400-nm region of the UV spectra (see Figures S2 and S3 in the Supporting Information). The relatively close stepwise constants for the successive formation of the mono- and binuclear species (entry 1 in Table 2 and entry 2 in Table 3) in comparison with L^3 again supports that both metal ions have almost independent binding sites in the macrocycle. The low pK_a values of the hydrolysis reactions $M_2L^{4+} + H_2O = M_2L(OH)^{3+} + H^+$ [pK_a = 7.4(1)] and $M_2L(OH)^{3+} + H_2O = M_2L(OH)_2^{2+} + H^+$ [pK_a = 8.61(4)] suggest that the hydroxido ligands bridge both metal centres. The most distinctive feature of L in relation to L^1, L^2 and L^3 is the formation of trinuclear species of the type $[Cu_3L(OH)_r]^{(6-r)+}$ (Table 4). For a 3:1 molar ratio, the trinuclear species prevail in solution above pH 7, with $[Cu_3L(OH)_3]^{3+}$ being the major species. The pH value at which these species are formed strongly suggests that the OH^- groups also bridge the metal centres in these trinuclear species (see Scheme 3B).

CO_2 Fixation

EMF Measurements on Ternary Systems

To check the capability of this new terpyridinophane for capturing carbon dioxide we first performed preliminary potentiometric studies on the ternary system Cu^{II}/L/carbonate. A solution containing Cu^{II} and L in molar ratios 1:1, 2:1 and 3:1 and Na_2CO_3 was brought to basic pH with NaOH and then titrated with a dilute solution of perchloric acid until it reached a pH of about 4. Direct binding of carbonate by the macrocycle in the absence of metal was investigated previously without detecting any significant interaction.

Cu^{II}/L/carbonate ternary mono- and binuclear complexes with the stoichiometries $[CuH_nL(CO_3)]^{(n-2)+}$ (n = 1–7) and $[Cu_2H_nL(CO_3)]^{(n+2)+}$ (n = 0 and 2–4) are formed (see Figure 4). Table 5 collects the stepwise constants that have been calculated taking into account the pH range of existence of the binary complexes and the protonation constants of carbonate.[15] The values obtained are high and imply an almost quantitative complexation of hydrogen carbonate. Above pH 10, where the dihydroxylated binuclear complex $[Cu_2L(OH)_2]^{2+}$ predominates, interaction with carbonate is no longer observed, therefore it seems that hydroxide binding effectively competes with carbonate. This reasoning can also explain why we have not found mixed species in the case of the trihydroxylated trinuclear species.

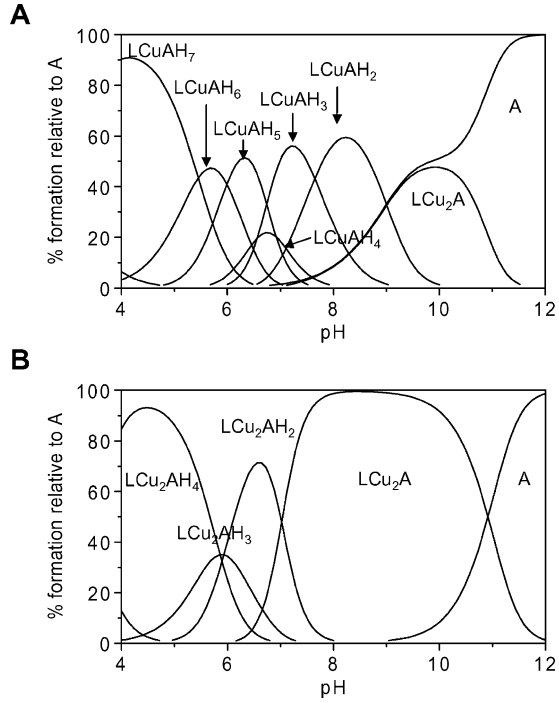

Figure 4. Distribution diagram for the ternary system Cu^{II}/L/A (A = carbonate): (A) molar ratio 1:1:1 $[Cu^{II}] = [L] = [A] = 10^{-3}$ M; (B) molar ratio 2:1:1 $[Cu^{II}] = 2 \times 10^{-3}$ M, $[L] = [A] = 10^{-3}$ M.

For a 1:1 Cu^{II}/L ration carbon dioxide fixation can be followed by UV spectroscopy. Since CO_2 absorption acidifies the solution, the exposure to the atmosphere of a 1:1 10^{-5} M solution of Cu^{II} and L yields an increase in the intensity of the UV bands at 330 and 340 nm (Figure 5).

Exposure to the atmosphere of an aqueous solution of $Cu(ClO_4)_2 \cdot 6H_2O$ and L in a 2:1 molar ratio at an initial pH of 9 leads, in a few minutes, to acidification of the solution, which reaches a pH of about 7.0. After a few hours blue crystals that unfortunately were not suitable for X-ray analysis were formed. However, FT-IR studies and elemental analysis of these crystals indicated that CO_2 fixation as carbonate had occurred.

Table 5. Selected logarithms of the stepwise formation constants for the system $Cu^{II}/L/A$ ($A = CO_3^{2-}$) determined at 298.1 ± 0.1 K in 0.15 M $NaClO_4$.

Entry	Reaction[a]	L	L^1[b]
1	$MH_5L + H_2A \leftrightarrows MH_7LA$	6.1(1)[c]	–
2	$MH_4L + H_2A \leftrightarrows MH_6LA$	5.7(1)	4.3(1)
3	$MH_5L + HA \leftrightarrows MH_6LA$	6.8(1)	5.7(1)
4	$MH_4L + HA \leftrightarrows MH_5LA$	6.0(1)	–
5	$MH_3L + HA \leftrightarrows MH_4LA$	5.1(2)	6.5(1)
6	$MH_2L + HA \leftrightarrows MH_3LA$	5.1(1)	5.9(1)
7	$MHL + HA \leftrightarrows MH_2LA$	5.01(6)	5.5(2)
8	$ML + HA \leftrightarrows MHLA$	4.83(6)	–
9	$M_2H_2L + H_2A \leftrightarrows M_2H_4LA$	6.4(1)	4.8(1)
10	$M_2H_2L + HA \leftrightarrows M_2H_3LA$	6.8 (2)	–
11	$M_2HL + H_2A \leftrightarrows M_2H_3LA$	6.5(2)	5.5(1)
12	$M_2HL + HA \leftrightarrows M_2H_2LA$	6.9(2)	7.1(1)
13	$M_2L(OH) + HA \leftrightarrows M_2LA$	6.7(2)	7.2(1)

[a] Charges omitted. [b] Values taken from ref.[5] [c] Values in parentheses are standard deviations in the last significant figure.

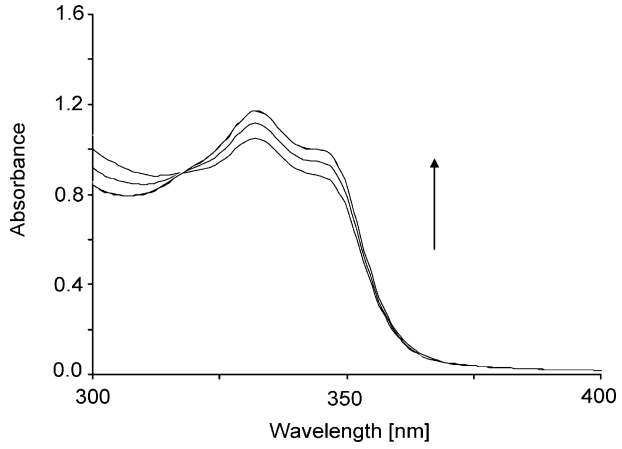

Figure 5. Electronic spectral change in the reaction of Cu^{II}/L with atmospheric CO_2 (in 0.15 M $NaClO_4$ at 298.1 K, [M] = [L] = 10^{-4} M). Repeated scans were initiated with a cycle time of 20 min immediately after exposure of the solution to air.

A plot of the absorbance at 340 nm against time shows a continuous increase of the absorbance until a plateau is observed after 60 min (Figure 6). This value improves the values (90 and 120 min) required for the systems Cu^{II}/L^1 and Zn^{II}/L^1, respectively, to achieve the same situation.

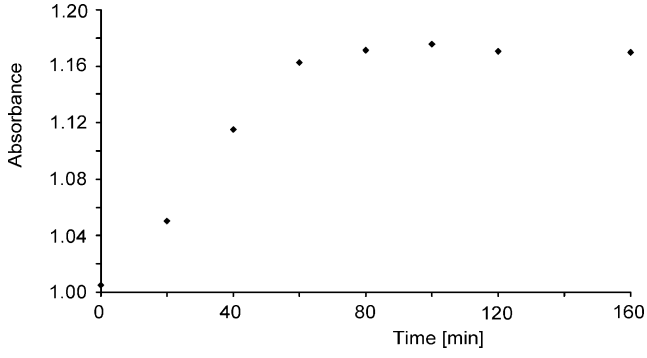

Figure 6. Evolution of the maximum of the band at 340 nm with time.

Paramagnetic NMR Spectroscopy

Paramagnetic ^1H NMR spectra were first recorded for the more simple ternary system $Cu_2/L^1/CO_2$ in order to compare them with the new terpyridinophane system $Cu_2/L/CO_2$. We recorded the paramagnetic ^1H NMR spectra, measured the ^1H longitudinal and transversal relaxation times (T_1 and T_2, respectively) and analyzed the temperature-dependence of the chemical shifts. The ^1H NMR spectrum of the dimer Cu_2/L^1 in D_2O at pH 9 is shown in Figure 7. The hyperfine-shifted resonances, linewidths at half-height, the T_1 values and the assignments of the isotropically shifted signals shown in Table 6 have been reported previously.[16]

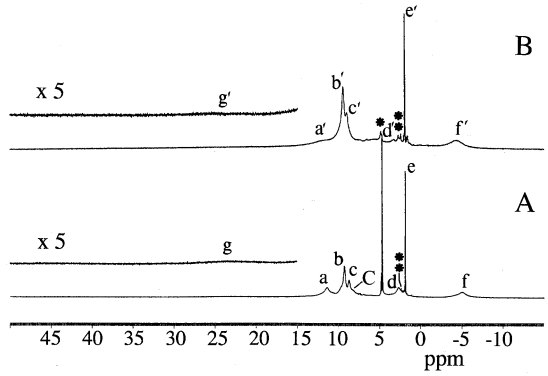

Figure 7. ^1H NMR spectra (400 MHz in D_2O at 298 K and pH 9) of Cu_2/L^1 (A) and $Cu_2/L^1/CO_3^{2-}$ (B). The asterisks indicate residual solvent and impurity signals (* H_2O, ** HOD).

When the spectrum of the ternary complex $Cu_2/L^1/CO_3^{2-}$ is recorded in D_2O at pH 9 a similar pattern of chemical shifts to that of the dimer appears (Figure 7B and Table 6). However, the NMR spectrum of the CO_3^{2-} complex is different to the spectrum of the dimer. Thus, some isotropic shifts in the downfield and upfield regions move by up to 0.7 ppm, except for signal e′, which is assigned to the $H_{m,p}$ terpyridine protons (see Scheme 4). Similarly, the narrower line widths of the paramagnetic signals (except signal a′) can be interpreted as being due to a change in the coordination geometry of the copper sites and therefore in the electronic properties of the metals ions in the ternary complex $Cu_2/L^1/CO_3^{2-}$. In addition, our results indicate that the coordination of a bridging carbonate ligand move the aliphatic chain with respect to the terpyridine group plane. These results are clearly consistent with the crystallographic studies published previously.[5] The magnitude of the deformation of the macrocyclic ring is less important in the carbonate complex than in the imidazole complex.[16]

Variable-temperature ^1H NMR spectra of the ternary complex $Cu_2/L^1/CO_3^{2-}$ were also registered between 283 and 323 K and the observed isotropically shifted resonances of protons were plotted as a function of the inverse of the temperature. Isotropically shifted signals are temperature dependent and follow an anti-Curie behaviour, except for some signals belong to α-CH_2 or the *ortho* phenyl protons

Table 6. ^{1}H NMR hyperfine-shifted resonances of Cu_2/L^1 and $Cu_2/L^1/CO_3^{2-}$ complexes in D_2O at 298 K and pH 9.

System	Signal	δ [ppm]	Number of protons	Assignment	Temp. dependence	T_1 [ms]	$\Delta\nu_{1/2}$ [Hz]	T_2[a] [ms]
Cu_2/L^1	a	11.4	12	α-CH_2	Curie	3.3	232	1.4
	d	2.6			anti-Curie	1.7	284	1.1
	f	–5.1			Curie	<1	911	0.35
	b	9.3	8	γ-CH_2	anti-Curie	3.2	179	1.8
	c	8.7	4	β-CH_2	anti-Curie	2.7	142	2.2
	C	8.1[b]			–	[c]	[c]	[c]
	e	1.9	7	$H_{m,p}$-Tpy	anti-Curie	66.5	9.6	33.2
	g	23.4	2	H_o-Tpy	Curie	<1	2323	0.14
$Cu_2/L^1/CO_3^{2-}$	a′	11.7	12	α-CH_2	Curie	2.5	585	0.54
	d′	3.2			anti-Curie	2.6	195	1.6
	f′	–4.4			Curie	<1	650	0.49
	b′	9.4	12	γ-CH_2	anti-Curie	2.7	170	1.9
	c′	9.0		β-CH_2	anti-Curie	2.4	[c]	[c]
	e′	1.9	7	$H_{m,p}$-Tpy	anti-Curie	163.9	6.0	53.1
	g′	24.0	2	H_o-Tpy	Curie	<1	2211	0.14

[a] Measured from the line width at half-height. [b] Measured at 313 K. [c] Overlap prevents measurement of this value.

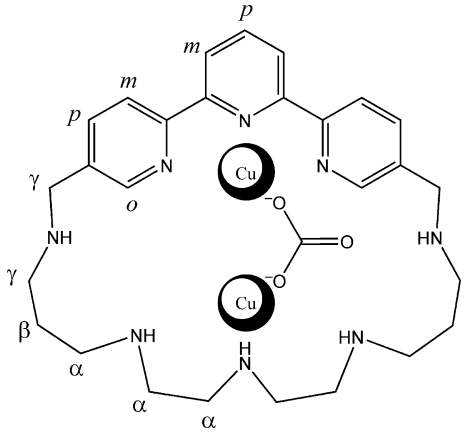

Scheme 4.

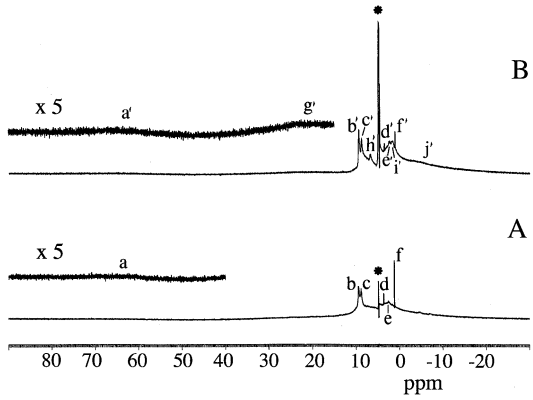

Figure 8. ^{1}H NMR spectra (400 MHz in D_2O at 298 K and pH 9) of Cu_2/L (A) and $Cu_2/L/CO_3^{2-}$ (B). The asterisks indicate residual solvent (*, H_2O).

of the macrocyclic ligand, which show a Curie behaviour where the paramagnetic shift signals increase with decreasing temperature (see Table 6). This anti-Curie behaviour is indicative of a spin-coupled Cu^{II}–Cu^{II} system with antiferromagnetic coupling.

The ^{1}H NMR spectra for the new terpyridinophane systems Cu_2/L and $Cu_2/L/CO_3^{2-}$ are shown in parts A and B of Figure 8 and the chemical shifts, ^{1}H longitudinal relaxation times and linewidths at half-height are listed in Table 7. The spectra show a similar pattern of hyperfine-shifted resonances to that seen in the spectrum of the dimer Cu_2/L^1 (see Figure 7A). The assignment of the isotropically shifted signals by means of the longitudinal relaxation times and the integration of paramagnetic signals is in close agreement with the ^{1}H NMR assignment of Cu_2/L^1 and $Cu_2/L^1/CO_3^{2-}$ discussed above (see the assignments for Cu_2/L and $Cu_2/L/CO_3^{2-}$ in Table 7 and Scheme 5).

We also observed a similar pattern of chemical shifts for the new terpyridinophane system $Cu_2/L/CO_3^{2-}$ to that seen in the spectrum of the binuclear complex Cu_2/L. However, several new signals (g′, h′, i′, j′) also appear in the ^{1}H NMR spectrum of the ternary system $Cu_2/L/CO_3^{2-}$ in D_2O at pH 9 (Figure 8B) and the peaks of some macrocyclic protons show linewidths, measured at half-height, that are up to 200 Hz narrower. We also observed a multiplet structure for the resonances of the aliphatic protons of the chains (α-CH_2, β-γ-CH_2). This behaviour can be related to a change in the structure of the complex triggered by the coordination of the carbonate ligand to the copper sites. Additionally, as mentioned above, the narrower line widths of the paramagnetic signals confirm the interaction of the binuclear Cu_2-L complex with carbonate ligand. Thus, our data clearly demonstrate the coordination of the bridging carbonate ligand.

Variable-temperature ^{1}H NMR studies of the ternary complex $Cu_2/L/CO_3^{2-}$ show that most of the isotropically shifted signals are temperature-dependent and follow an anti-Curie behaviour, although some signals belonging to the α-CH_2 group or the *ortho* phenyl protons of the macrocyclic ligand show a Curie behaviour (see Table 7). These results again confirm the existence of a spin-coupled Cu^{II}–Cu^{II} system with antiferromagnetic coupling.

Table 7. ^1H NMR hyperfine-shifted resonances of Cu_2/L and $Cu_2/L/CO_3^{2-}$ complexes in D_2O at 298 K and pH 9.

System	Signal	δ [ppm]	Number of protons	Assignment	Temp. dependence	T_1 [ms]	$\Delta\nu_{1/2}$ [Hz]	T_2[a] [ms]
Cu_2/L	a	62.5	2	H_o-Tpy	Curie	<1	4560	0.07
	b	9.3	10	β-γCH_2	*T*-independent	4.4	175	1.8
	c	8.8			anti-Curie	5.6	175	1.8
	d	3.5	6	δ-εCH_2	anti-Curie	186.7	7.0	45.5
	e	2.5	12	α-CH_2	anti-Curie	[b]	[b]	[b]
	f	1.1	7	$H_{m,p}$-Tpy	anti-Curie	212.6	9.0	35.4
$Cu_2/L/CO_3^{2-}$	a′	64.0	2	H_o-Tpy	Curie	<1	4320	0.07
	b′	9.4	10	β-γCH_2	*T*-independent	4.7	133	2.4
	c′	8.8			anti-Curie	4.9	130	2.4
	h′	6.8			anti-Curie	6.1	110	2.9
	d′	3.5	6	δ-εCH_2	anti-Curie	154	16	19.9
	e′	2.5	12	αCH_2	anti-Curie	[b]	[b]	[b]
	i′	1.6			anti-Curie	[b]	[b]	[b]
	g′	23.0			Curie	<1	2400	0.13
	j′	–4.0			Curie	<1	1440	0.22
	f′	1.1	7	$H_{m,p}$-Tpy	anti-Curie	141	18	17.7

[a] Measured from the line width at half-height. [b] Overlap prevents measurement of this value.

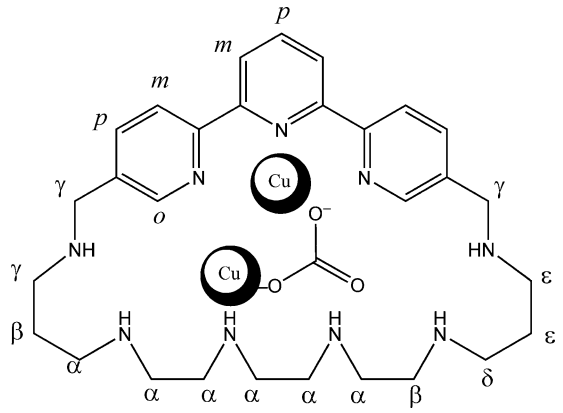

Scheme 5.

Electrochemistry

The response of Cu^{II}/L binary solutions is similar to that described previously for the Cu^{II}/L^1 system.[5] The copper complexes studied here are reduced in two successive one-electron processes that form successively a Cu^I/L complex and Cu metal at + 0.15 and –0.20 V vs. AgCl/Ag, respectively. The overall two-electron reduction process was confirmed by EQCM measurements. A unique reduction peak appears at –0.53 V upon exposure to air and is followed by a significant increase of the current at potentials above –1.0 V. This effect is observed even for low complex concentrations, as can be seen in Figure 9. Upon bubbling CO_2 through the electrochemical cell, the voltammograms exhibit a clear increase of the reduction current between –1.0 and –1.25 V with time, which is attributable to the complex-catalyzed reduction of CO_2.

The voltammetric response observed in ternary $Cu^{II}/L/CO_2$ solutions can be rationalized, as previously discussed,[5] in terms of an inner-sphere pathway involving the formation of Cu^{II}/L/carbonate ternary complexes, which means that CO_2 reduction presumably occurs at a potential corresponding to the redox potential of an adduct formed between the reduced substrate and the catalyst.[17–21] Taking into account our previous results with the analogous ligand L^1, CO_2 will most likely be bound as carbamate in the mixed complexes. Carbamate formation is also supported by the FAB mass spectra of aqueous solutions containing either Cu^{II} and L·8 HBr exposed to air or Cu^{II}, L·8 HBr and added sodium hydrogen carbonate, both with a final pH of 6.8. The spectra of both solutions − the one containing added hydrogen carbonate and the one exposed to the

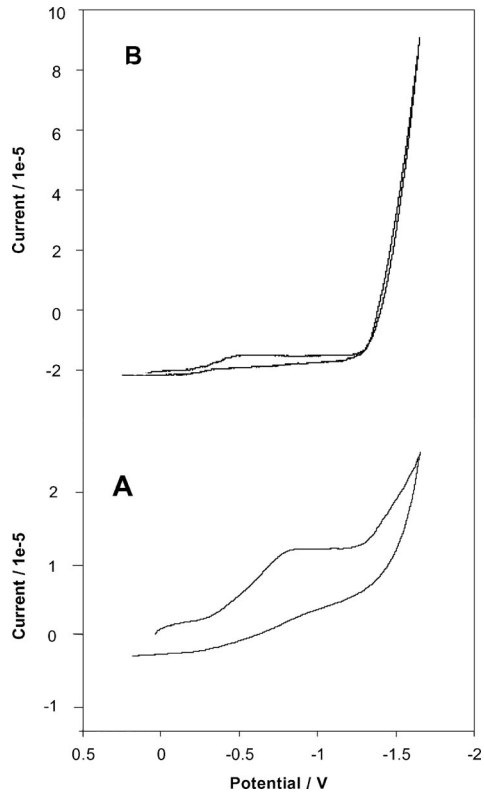

Figure 9. CVs at a GCE for a 2×10^{-5} M solution of Cu^{II}/L (A) and a 1×10^{-5} M solution of Cu^{II}/L (B) after exposition to air for 60 min. Electrolyte: 0.15 M $NaClO_4$. Potential scan rate: 100 mV s^{-1}.

atmosphere – show the presence of a peak at *m*/*z* 566 attributable to the ionic species $[Cu(H_3L)(carb)Na_2Br_2(ClO_4)_3]^{2+}$. Additionally, in the solution containing Cu^{II}, L·8HBr and added sodium hydrogen carbonate there is a peak at *m*/*z* 746 that can be attributed to the species $[Cu(H_{-1}L)(carb)NaClO_4]^{+}$.

To test the possibility of an electrochemically promoted activation of CO_2, the electrochemistry of Cu^{II}/L^1 solutions at indigo-modified FTOs was studied. Figure 10A shows the voltammetry of indigo microparticles in contact with CO_2-saturated acetate buffer in the presence of 10^{-3} M $CuSO_4 \cdot 5H_2O$. This voltammetry is essentially identical to that obtained at indigo-modified electrodes in the absence of Cu^{II} ions and/or CO_2 and consists of two well-defined peaks at +0.47 and –0.28 V vs. AgCl/Ag. According to the literature, these peaks correspond to the two-electron, two-proton oxidation of indigo to dehydroindig, and the two-electron, two-proton reduction of indigo to leucoindigo, respectively.[7–9] These processes can be represented as depicted in Scheme 6.

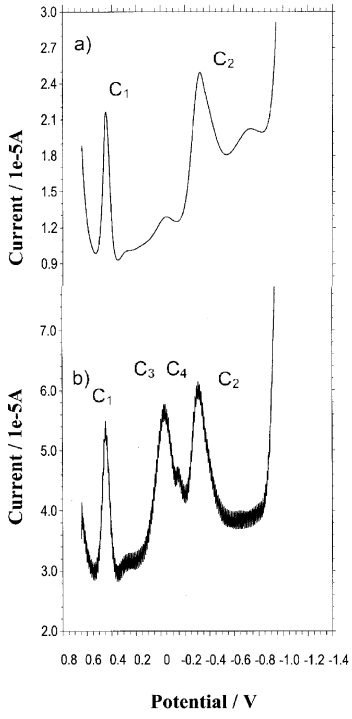

Figure 10. SQWVs of indigo-modified PIGEs immersed in CO_2-saturated 0.25 M acetic acid + 0.25 M sodium acetate solutions containing: a) 1×10^{-3} M Cu^{II}; b) 1×10^{-3} M Cu^{II} + 1×10^{-3} M L^1. Potential scan initiated at +0.65 V in the negative direction after an electrogeneration step performed by applying a constant potential of –1.45 V for 5 min. Potential step increment: 4 mV; square wave amplitude: 25 mV; frequency: 5 Hz.

Significant changes were detected in the voltammograms in the presence of Cu^{II} and L^1 in a 1:1 molar ratio, where two additional peaks at –0.03 (C^3) and –0.15 V (C^4) accompany signals C^1 and C^2. These signals are increase notably after applying an electrogeneration step consisting of the application of a constant potential between –1.45 and –1.65 V for periods of time of between 1 and 15 min, as shown in part B of Figure 10. Such additional peaks are enhanced on increasing the Cu^{II}+ligand concentrations in the 10^{-5} to 10^{-3} M range.

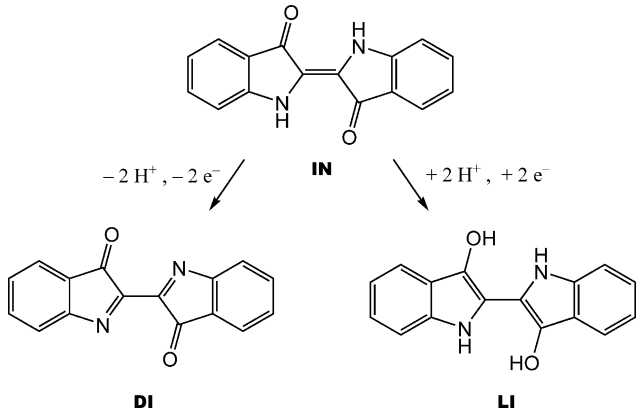

Scheme 6. Redox processes involving indigo (IN), dehydroindigo (DI) and leucoindigo (LI).

This electrochemical response can be described in terms of the activation of CO_2 by formation of Cu^{II}/L^1/carbamate complexes. The reduction of carbon dioxide at inert electrodes proceeds by the mechanism suggested by Amatore and Saveant in which carbon monoxide, carbonate and oxalate ions can be formed through disproportionation or dimerization of the radical anion produced in the initial one-electron reduction of carbon dioxide [see Equations (1), (2), (3) and (4)].[17]

$$CO_2 + e^- \rightarrow CO_2^{\cdot -} \quad (1)$$

$$2CO_2^{\cdot -} \rightarrow CO + CO_3^{2-} \quad (2)$$

$$2CO_2^{\cdot -} \rightarrow C_2O_4^{2-} \quad (3)$$

$$CO_2^{\cdot -} + H^+ + e^- \rightarrow HCOO^- \quad (4)$$

The formation of active $CO_2^{\cdot -}$ radical anion is catalyzed by the Cu^{II}/L^1 complex, which promotes the formation of the indigo-carboxylated compounds that are responsible for the electrochemical processes C^3 and C^4. First of all, the appearance of new reduction peaks suggests that a simple outer-sphere electron transfer between any indigo form and the radical anion does not occur. As previously described, the catalytic reduction potential of CO_2 is considerably more negative than the formal reduction potential of the catalyst and it is likely that CO_2 reduction occurs at a potential corresponding to the redox potential of an adduct formed between the reduced substrate and the catalyst. Under our experimental conditions, the Cu^{II}/L^1 complex catalyzes the initial one-electron reduction of CO_2, thus producing the "active" $CO_2A^{\cdot -}$ radical anion.

To verify the effectiveness of the carboxylation process, FTIR-ATR spectra of materials deposited on indigo-modified FTOs were recorded at different stages during the electrochemical turnovers. The FTIR-ATR spectra of the parent indigo-modified electrode and that resulting after appli-

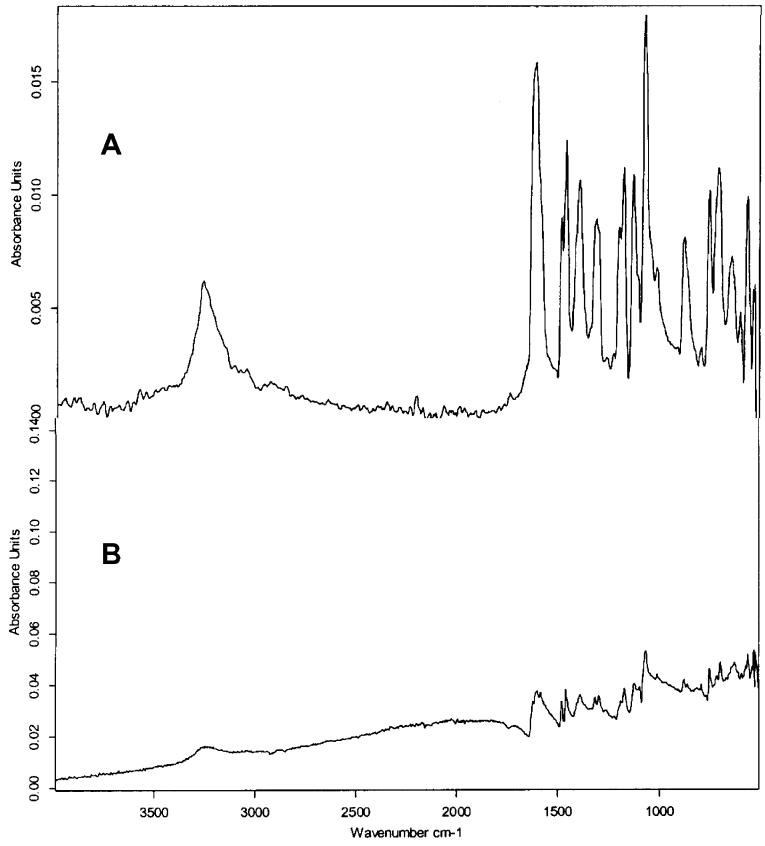

Figure 11. FTIR-ATR spectra of an indigo-modified FTO electrode before (a) and after (b) application of a constant potential of –1.45 V during 10 min in a 0.50 mM Cu^{II} + 0.50 mM L^1 CO_2-saturated solution in 0.50 M acetate buffer.

cation of a constant potential of –1.45 V for 10 min in a 0.50 mM Cu^{II} + 0.50 mM L^1 CO_2-saturated solution in 0.50 M acetate buffer are compared in Figure 11.

The FTIR-ATR spectrum of indigo (Figure 11A) shows a characteristic carbonyl band at 1635 cm^{-1} accompanied by typical aromatic bands, the alkene band at 1650 cm^{-1}, and amine bands at about 3500 cm^{-1}. After the above-described electrogeneration step (Figure 11B), the spectrum exhibits a well-defined band at 1060 cm^{-1}, which is assigned to the alcohol C–O vibration, and a band at 1720 cm^{-1} whose profile is characteristic of carboxylate groups. The bands at 1635 and 1650 cm^{-1} disappear, which indicates the absence of carbonyl and conjugated alkene units, as can be seen in the detailed reflectance-mode spectrum depicted in Figure 12.

The observed electrochemistry can tentatively be described in terms of attack at the C=C bonds of leucoindigo by $CO_2A^{\cdot-}$, both of which are electrochemically generated, to give a carboxylated indigo derivative [Equation (5):

$$H_4IN\ (s) + 2CO_2A^{\cdot-}\ (aq) \rightarrow H_4IN(COO^-)_2\ (s) \quad (5)$$

In agreement with this proposal, reduction peaks C^3 and C^4 fall in the typical potential range where the reduction of indigo derivatives occurs.[22,23] A possible reaction pathway for explaining the Cu^{II}/L^1-catalyzed electrochemical activation of indigo carboxylation is shown in Scheme 7.

To verify the solid-state reactivity, electrochemical CO_2 activation catalyzed by Cu^{II}/L^1 was performed in the electrochemical AFM cell. Isolated indigo grains were deposited onto a graphite plate and submitted to different electrochemical cycles after immersion into complex-containing CO_2-saturated solution in acetate buffer. The AFM images recorded at different applied potentials are shown in Figure 13. At zero applied potential (Figure 13A), irregular isolated indigo aggregates appear, whereas at potentials of around –0.5 V, a deposit of metallic copper, consisting of multiple grains, is formed (Figure 13B). At potentials between –1.0 and –1.5 V the deposit of copper metal redissolves while the indigo aggregates appear to undergo some morphological changes (Figure 13C). This effect, which denotes the existence of a solid-state reaction, can be more clearly seen in the AFM images in Figure 14. These images reveal a significant enlargement of the grain, which is attributable to the formation of a layer of carboxylated derivative(s).

These features can be considered in the light of models for the electrochemistry of insertion solids proposed by Lovric, Scholz and Oldham et al.[24–27] Following this scheme, the redox reaction for indigo microparticles is initiated at the three-phase electrode/electrolyte/microparticle junction and expands by proton transfer across the electrolyte/particle interface and electron transfer across the electrode/particle interface.

The situation is more complicated here, however, because carboxylation must occur at least on the more external surface of the indigo particles. A pictorial representation is de-

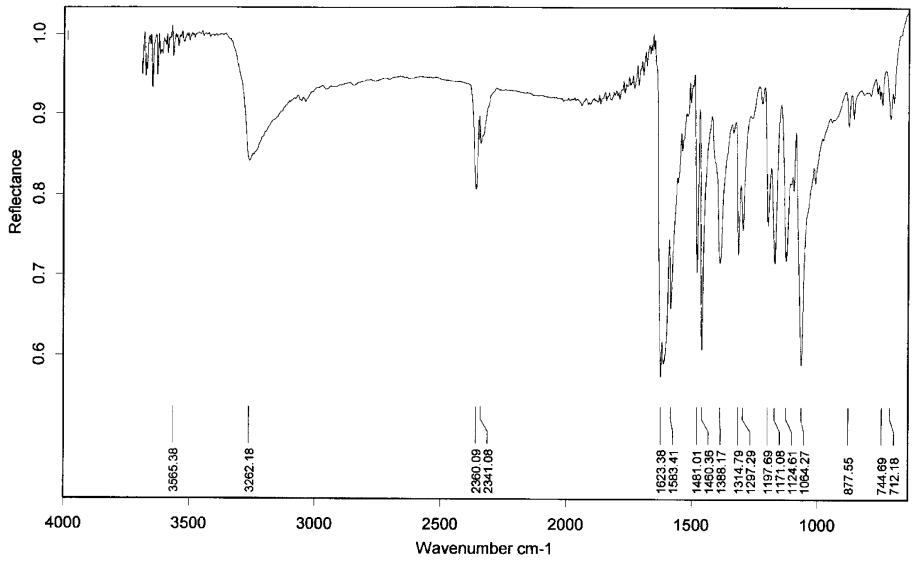

Figure 12. Detail of the FTIR-ATR spectrum ofr an indigo-modified FTO electrode submitted to an electrogeneration step of –1.45 V for 10 min in a 0.50 mM Cu^{II} + 0.50 mM L^1 CO_2-saturated solution in 0.50 M acetate buffer.

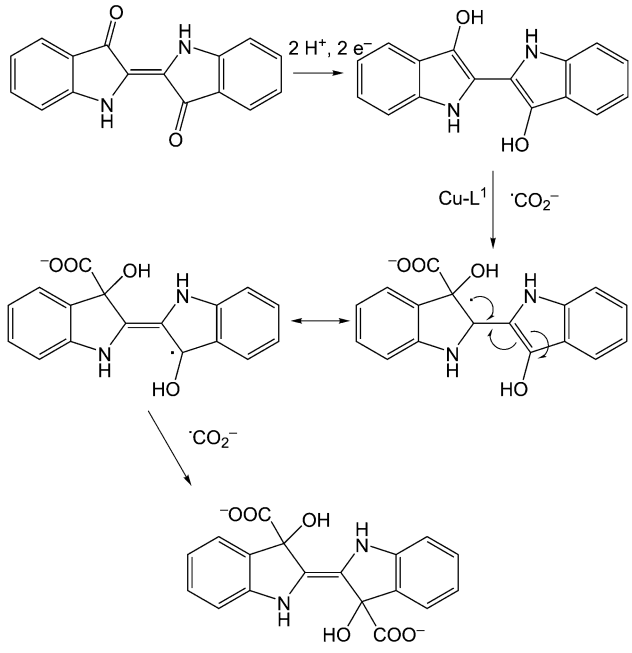

Scheme 7. Possible reaction pathway for the carboxylation of indigo.

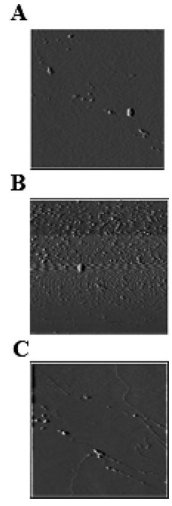

Figure 13. AFM images recorded at different potentials applied to a deposit of indigo grains in contact with a CO_2-saturated solution containing 0.10 mM Cu^{II}/L^1 complex in 0.50 M acetate buffer: a) open-circuit conditions; b) –0.55 V; c) –1.25 V. Image size: 10 μm.

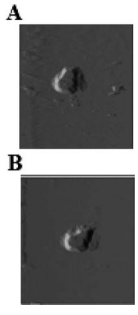

Figure 14. AFM image of an indigo grain in contact with CO_2-saturated solution containing 0.10 mM Cu^{II}/L^1 complex in 0.50 M acetate buffer: a) open-circuit conditions; b) after applying a constant potential of –1.5 V for 5 min. Image size: 2 μm.

picted in Scheme 8. Accordingly, electrochemically assisted carboxylation of indigo proceeds initially by proton insertion coupled with electron hopping, which results in the formation of solid leucoindigo (Scheme 8) followed by the carboxylation reaction [Equation (5)]. This carboxylation proceeds throughout the indigo particle and involves diffusion of $CO_2A^{\cdot-}$ units and bond rearrangement through leucoindigo molecules. This process is prompted by the more flexible nature of leucoindigo molecules, which have a central single C–C bond (see Scheme 6), with respect to the parent indigo ones, which have a central C=C double bond. Solid-state reactions prompted by the flexible nature

of molecules can cause topochemical transformations to proceed with minimal distortion of the crystal lattice, as described by Kim et al. for Diels–Alder cycloadditions in the solid state.[28]

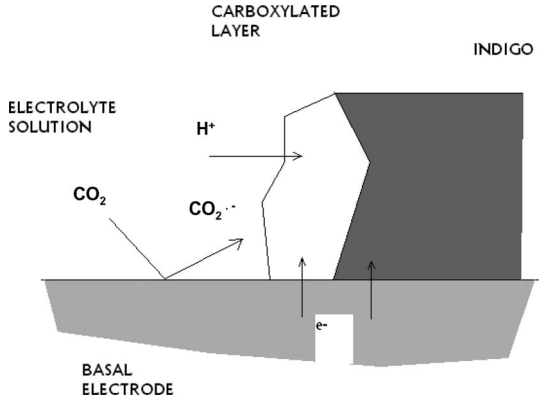

Scheme 8. Pictorial representation of the solid-state electrochemically assisted carboxylation of indigo microparticles deposited on an FTO electrode.

Conclusions

Synthesis of the new terpyridinophane L, which is obtained by cyclisation of 5,5′′-bis(bromomethyl)-2,2′:6′,2′′-terpyridine with 1,5,8,11,14,18-hexakis(*p*-tolylsulfonyl)-1,5,8,11,14,18-hexaazaoctadecane followed by detosylation with HBr/HOAc/PhOH, has been reported. L interacts with Cu^{II} to form mono- and binuclear complexes as well as trinuclear trihydroxylated species. L is also able to interact with atmospheric CO_2 faster than the previously reported terpyridinophane L[1]. The stability constants of the mixed complexes denote quantitative formation of the Cu^{II}/L/carbonate complexes in a wide pH range. Finally, the electrochemical activation of CO_2 and its incorporation into a solid state sample of indigo dye has been shown.

Experimental Section

Synthesis of L: 5,5′′-Bis(bromomethyl)-2,2′:6′,2′′-terpyridine (**1**)[29] and 1,5,8,11,14,18-hexakis(*p*-tolylsulfonyl)-1,5,8,11,14,18-hexaazaoctadecane (**2**)[6] were prepared as described previously. The other chemicals were used as purchased without further purification. CH_3CN was dried with 3-Å molecular sieves. CH_2Cl_2 was distilled from CaH_2 prior to use. Column chromatography was performed with aluminum oxide (neutral, SDS). Aluminium oxide 60 F_{254} neutral (Merck) plates were used for TLC.

2,6,9,12,15,19-Hexakis(*p*-tolylsulfonyl)-2,6,9,12,15,19-hexaaza[20]-(5,5′′)-terpyridinocyclophane (L·6Ts): 5,5′′-Bis(bromomethyl)-2,2′:6′,2′′-terpyridine (**1**; 0.315 g, 0.75 mmol) in dry CH_2Cl_2 (30 mL) was slowly added dropwise to a mixture of **2** (0.89 g, 0.75 mmol) and K_2CO_3 (1.04 g, 7.5 mmol) in refluxing CH_3CN (50 mL). Once the addition was complete, most of the CH_2Cl_2 was distilled off and the remaining mixture was refluxed under argon for 20 h. The reaction mixture was then filtered through paper while hot and the solid washed thoroughly with CH_3CN. The combined organic layers were concentrated in vacuo to yield a yellow solid (0.88 g), which was submitted to column chromatography on alumina (CH_2Cl_2, 0 to 5% EtOAc as eluent) to afford **L**·6Ts (0.44 g, 41%) as a white solid. ^{1}H NMR ($CDCl_3$, 300 MHz): δ = 8.62–8.59 (m, 4 H), 8.31 (d, J = 7.7 Hz, 2 H), 7.96 (dd, J = 8.3 and 2.1 Hz, 2 H), 7.81 (t, J = 7.7 Hz, 1 H), 7.78 (d, J = 8.3 Hz, 4 H), 7.64 (d, J = 8.3 Hz, 4 H), 7.57 (d, J = 8.3 Hz, 4 H), 7.39 (d, J = 8.3 Hz, 4 H), 7.33 (d, J = 8.3 Hz, 4 H), 7.24 (d, J = 8.3 Hz, 4 H), 4.28 (br. s, 4 H), 3.16–3.09 (m, 4 H), 2.99–2.86 (m, 8 H), 2.80–2.68 (m, 8 H), 2.48 (s, 6 H), 2.45 (s, 6 H), 2.38 (s, 6 H), 1.70–1.61 (m, 4 H) ppm. ^{13}C NMR ($CDCl_3$, 75.43 MHz): δ = 155.6, 154.5, 149.3, 144.0, 143.8, 143.6, 137.9, 137.5, 135.2, 135.0, 134.9, 132.9, 130.1, 129.9, 127.5, 127.4, 121.4, 121.1, 52.0, 49.0, 48.6, 48.4, 48.1, 48.0, 29.8, 21.7, 21.6 ppm.

2,6,9,12,15,19-Hexaaza[20]-(5,5′′)-terpyridinocyclophane Octabromohydrate (L·8HBr): The tosyl groups of L·6Ts (0.380 g, 0.263 mmol) were removed by reductive cleavage with a mixture of 20 mL of HBr/HOAc and PhOH (1.89 g, 20.1 mmol) by heating at 90 °C for 24 h. The solid obtained was filtered off and washed with a mixture of EtOH and CH_2Cl_2 (1:1) to give the macrocycle as its hydrobromide salt (0.240 g). Yield 97%. ^{1}H NMR (D_2O, 300 MHz): δ = 9.06 (d, J = 1.9 Hz, 2 H), 8.68 (d, J = 8.3 Hz, 2 H), 8.54 (dd, J = 8.3 and 1.9 Hz, 2 H), 8.50 (d, J = 7.1 Hz, 2 H), 8.38 (dd, J = 7.1 and 6.8 Hz, 1 H), 4.60 (s, 4 H), 3.50 (br. s, 4 H), 3.48–3.45 (m, 8 H), 3.29–3.17 (m, 8 H), 2.19–2.09 (m, 4 H) ppm. ^{13}C NMR (D_2O, 75.43 MHz): δ = 152.1, 151.3, 148.0, 145.2, 141.7, 129.0, 125.0, 124.7, 47.5, 45.1, 43.4, 43.3, 43.1, 30.5, 23.0 ppm. $C_{29}H_{43}N_9$·8HBr (1156.8): calcd. C 30.1, H 4.4, N 10.9; found C 30.3, H 4.6, N 11.0.

EMF Measurements: The potentiometric titrations were carried out at 298.1 ± 0.1 K using 0.15 M $NaClO_4$ as supporting electrolyte. The experimental set-up (burette, potentiometer, cell, stirrer, microcomputer, etc.) has been fully described elsewhere.[30] The EMF data were acquired with the computer program PASAT.[31] The reference electrode was a Ag/AgCl electrode in saturated KCl solution. The glass electrode was calibrated as a hydrogen-ion concentration probe by titration of previously standardized amounts of HCl with CO_2-free NaOH solutions and the equivalent point determined by Gran's method,[32] which gives the standard potential, $E°'$, and the ionic product of water [pK_w = 13.73(1)].

The computer program HYPERQUAD was used to calculate the protonation and stability constants.[10] The pH range investigated was 2.5–11.0 and the concentration of the metal ions and of the ligands ranged from 1×10^{-3} to 5×10^{-3} M with M/L molar ratios varying from 3:1 to 1:2. For the ternary systems, aqueous solutions at basic pH containing M/L in 1:1 and 2:1 molar ratios and different amounts of Na_2CO_3 were titrated with $HClO_4$ solutions. The different titration curves for each system (at least two) were treated either as a single set or as separate curves without significant variations in the values of the stability constants. Finally, the data sets were merged together and treated simultaneously to give the final stability constants.

Spectrophotometric Titrations: Absorption spectra were recorded with a Shimadzu UV-2501PC spectrophotometer. HCl and NaOH were used to adjust the pH values, which were recorded with a Meterlab PHM240 Radiometer pH meter.

Paramagnetic NMR Spectroscopy: ^{1}H NMR spectra were recorded with a Bruker Avance400 spectrometer operating at 399.91 MHz. One-dimensional spectra were recorded in D_2O solvent with presaturation of the H_2O signal during part of the relaxation delay to eliminate the H_2O signal. Relaxation delay times of 50–400 ms, spectral widths of 40–80 kHz and acquisition times of 60–400 ms were used. 1D spectra were processed using exponential line-broad-

ening weighting functions as apodization with values of 10–40 Hz. Chemical shifts were referenced to the residual solvent protons of D_2O resonating at $\delta = 4.76$ ppm (298 K) relative to TMS. The longitudinal relaxation times of the hyperfine-shifted resonances were determined using the inversion recovery pulse sequence (d_1–180°–τ–90°–acq)[33] with 14 values of τ between 0.5 ms and 500 ms, (d_1+acq) values of at least five times the longest expected T_1 (ranging from 100 to 800 ms), and a total number of scans of 7000. The T_1 values were calculated from the inversion-recovery equation. Transversal relaxation times were obtained by measuring the line broadening of the isotropically shifted signals at half-height with the equation $T_2^{-1} = \pi\Delta\nu_{1/2}$.

Electrochemical Measurements: Linear potential scan, cyclic and square-wave voltammetric experiments (LSV, CV, and SQWV, respectively) were performed on aqueous solutions (0.15 M $NaClO_4$) of $Cu(NO_3)_2{\cdot}6H_2O$ (10^{-3} M; from Merck) containing a stoichiometric amount or a small excess of the macrocyclic ligand. To study the electrochemistry of binary metal-macrocycle complexes, equimolar amounts of metal nitrate and the ligand were dissolved in 0.15 M $NaClO_4$, which had previously been degassed with argon, and then voltammograms were recorded. To study the ternary Cu^{II}/L/carbonate complexes, the metal-receptor solution was exposed to air with stirring for between 30 min and 6 h; the resulting solution was then degasified by bubbling argon for 10 min and then the voltammograms were recorded. The pH was adjusted to the required values by adding appropriate amounts of aq. $HClO_4$ and/or NaOH solutions.

Electrochemical experiments were performed with a BAS CV 50W or CH I420 apparatus in a conventional three-compartment cell with glassy carbon and gold working electrodes. The working electrode was cleaned and activated prior to each series of experiments. Electrochemical pre-treatment was performed by adapting the procedure recommended by Engstrom and Strasser,[34] in blank solutions by applying +1.50 V vs. AgCl/Ag for 10 min followed by –1.0 V for 1 min. The electrodes were polished with an aqueous suspension of alumina on a soft surface then dried and cleaned before each run. An AgCl (3 M NaCl)/Ag and a platinum wire auxiliary electrode completed the three-electrode configuration. Semiderivative convolution of data was used to increase peak resolution in some cases. Experiments on indigo coatings on fluorine-doped tin oxide electrodes (FTOs, Flexitec 45) were performed using uniform deposits of indigo prepared by reported sonoelectrochemical procedures[35,36] by ultrasonication of the electrode immersed in a suspension (1 mg mL^{-1}) of indigo (Fluka) in acetone for 10 min. The electrode was then rinsed with water and dried in air. Polymer film electrodes were prepared, as described previously,[37] by transferring a small volume (typically 50 μL) of a dispersion of the solid (10 mg) in acetone (5 mL) to the surface of FTO and allowing the coating to dry in air. One drop of a solution of Paraloid B72 acrylic resin (1%) in acetone was then added and the modified electrode was air-dried.

FTIR-ATR spectra of indigo-modified electrodes were obtained with a Vertex 70 Fourier transform infrared spectrometer with a FR-DTGS (fast recovery deuterated triglycine sulfate) temperature-stabilized coated detector. Number of co-added scans: 32; resolution: 4 cm^{-1}.

Coupling voltammetric/atomic force microscopy experiments were performed with a Multimode AFM (Digital Instruments VEECO Methodology Group, USA) fitted with a NanoScope IIIa controller and equipped with a J-type scanner (max. scan size of 150×150×6 μm). The topography of the samples was studied in contact mode. An oxide-sharpened silicon nitride probe (Olympus, VEECO Methodology Group, model NP-S) was used with a V-shaped cantilever configuration (spring constant: 0.06 N m^{-1}; tip radius of curvature: 5–40 nm). The AFM was coupled to a Digital Instruments Universal Bipotentiostat (VEECO Methodology group, USA) for electrochemical measurements. All measurements were performed at room temperature in solutions previously deaerated with argon for 15 min.

Supporting Information (see footnote on the first page of this article): Figure S1. Distribution diagram for the system H^+-L. Figure S2. pH-dependence of the absorption spectra of Cu^{II}/L in a 2:1 M/L molar ratio. Figure S3. pH-dependence of the absorption spectra of Cu^{II}/L in a 3:1 M/L molar ratio. Table S1. Complete stability constants for the mononuclear copper complexes of the receptors L, L^1, L^2 and L^3. Table S2. Complete stability constants for the binuclear copper complexes of the receptors L, L^1, L^2 and L^3. Table S3. Cumulative stability formation constants for the systems Cu^{II}/L/carbonate and Cu^{II}/L^1/carbonate. Table S4 Most significant peaks observed in the FAB mass spectra of aqueous solutions containing either Cu^{II} and L·8HBr exposed to the atmosphere or Cu^{II}, L·8HBr and added sodium hydrogen carbonate, both with a final pH of 6.8.

Acknowledgments

Financial support from the Spanish Dirección General de Investigación Ciencia y Técnica (DGICYT) [grant nos. CTQ2006-15672-CO5-01/BQU and CTQ2006-15672-C05-05/BQU, both assisted by Fondo Europeo de Desarollo Regional (FEDER)] is gratefully acknowledged. S. B. and S. T. thank the Spanish Ministerio de Ciencia y Tecnología (MCYT) for PhD grants.

[1] a) G. Kolks, S. J. Lippard, J. V. Waszczak, *J. Am. Chem. Soc.* **1980**, *102*, 4832–4833; b) N. Kitajima, S. Hikichi, M. Tanka, M. Moro-oka, *J. Am. Chem. Soc.* **1993**, *115*, 5496–5508; c) C. Bazzicalupi, A. Bencini, A. Bianchi, F. Corana, V. Fusi, C. Giorgi, P. Paoli, P. Paoletti, B. Valtancoli, C. Zanchini, *Inorg. Chem.* **1996**, *35*, 5540–5548; d) A. Escuer, F. A. Mautner, E. Peñalba, R. Vicente, *Inorg. Chem.* **1998**, *37*, 4190–4196; e) P. Cocoloios, R. Guilard, D. Bayeul, C. Lecomte, *Inorg. Chem.* **1985**, *24*, 2058–2062. For reviews on related topics see: f) D. Walther, M. Ruben, S. Rau, *Coord. Chem. Rev.* **1999**, *182*, 67–100.

[2] a) H. Arakawa, M. Aresta, J. N. Armor, M. A. Barteau, E. J. Beckham, A. T. Bell, J. E. Bercraw, C. Creutz, E. Dinjus, D. A. Dixon, K. Domen, D. L. Dubois, J. Eckert, E. Fujita, D. H. Dibson, W. Goddard, D. W. Goodman, J. Keller, G. J. Kubas, H. H. Kung, J. Lyons, L. E. Manzer, T. J. Marks, K. Morokuma, K. M. Nicholas, R. Periana, L. Que, J. Rostrup-Nielsen, W. M. H. Sachtler, L. D. Schmidt, A. D. Sen, G. A. Somorjal, P. C. Stair, B. R. Stults, W. Tumas, *Chem. Rev.* **2001**, *101*, 953–996; b) I. Castro-Rodríguez, H. Nakai, L. N. Zakharov, A. L. Rheingold, K. Meyer, *Science* **2004**, *305*, 1757–1759; c) D. Santamaría, J. Cano, P. Royo, M. E. G. Mosquera, T. Cuenca, L. M. Frutos, O. Castano, *Angew. Chem. Int. Ed.* **2005**, *44*, 5828–5830; d) K. Mori, Y. Mitani, T. Hara, T. Mizugaki, K. Ebitani, K. Kaneda, *Chem. Commun.* **2005**, 3331–3333; e) L.-Y. Kong, Z.-H. Zhang, H.-F. Zhu, H. Kawaguchi, T.-A. Okamura, M. Doi, Q. Chu, W.-Y. Sun, N. Ueyama, *Angew. Chem. Int. Ed.* **2005**, *44*, 4352–4355; f) J.-L. Jiang, F. Gao, R. Hua, X. Jiu, *J. Org. Chem.* **2005**, *70*, 381–383; g) T. Bok, H. Yun, B. Y. Lee, *Inorg. Chem.* **2006**, *45*, 4228–4237; h) S. Schenck, J. Notni, U. Köhn, K. Wermann, E. Anders, *Dalton Trans.* **2006**, 4191–4206.

[3] a) D. B. Knaff, *Trends Biochem. Sci.* **1989**, *14*, 433–434; b) L. Stryer, *Biochemistry*, 4th Ed., W. Freeman Company, **1995**; c) W. Kaim, B. Schwederski, *Bioinorganic Chemistry; Inorganic*

Elements in the Chemistry of Life, An Introduction and Guide, J. Wiley and Sons, Chichester, **1995**.
[4] E. García-España, P. Gaviña, J. Latorre, C. Soriano, B. Verdejo, *J. Am. Chem. Soc.* **2004**, *126*, 5082–5083.
[5] B. Verdejo, J. Aguilar, E. García-España, P. Gaviña, J. Latorre, C. Soriano, J. M. Llinares, A. Doménech, *Inorg. Chem.* **2006**, *45*, 3803–3815.
[6] J. Aguilar, P. Díaz, F. Escartí, E. García-España, L. Gil, C. Soriano, B. Verdejo, *Inorg. Chim. Acta* **2002**, *339*, 307–316.
[7] A. M. Bond, F. Marken, E. Hill, R. G. Compton, H. Hügel, *J. Chem. Soc. Perkin Trans. 2* **1997**, 1735–1742.
[8] T. Grygar, S. Kuckova, D. Hradil, D. Hradilova, *J. Solid State Electrochem.* **2003**, *7*, 706–713.
[9] A. Doménech, M. T. Doménech, *J. Solid State Electrochem.* **2006**, *10*, 459–470.
[10] P. Gans, A. Sabatini, A. Vacca, *Talanta* **1996**, *43*, 1739–1753.
[11] J. Aguilar, M. G. Basallote, L. Gil, M. A. Mañez, E. García-España, C. Soriano, B. Verdejo, *Dalton Trans.* **2004**, 94–103.
[12] A. Bencini, A. Bianchi, E. García-España, J. A. Ramírez, *Coord. Chem. Rev.* **1999**, *188*, 97–136.
[13] C. Bazzicalupi, A. Bencini, E. Berni, A. Bianchi, A. Danesi, C. Giorgi, B. Valtancoli, C. Lodeiro, J. C. Lima, F. Pina, M. A. Bernardo, *Inorg. Chem.* **2004**, *43*, 5134–5146.
[14] A. Mendoza, J. Aguilar, M. G. Basallote, L. Gil, J. C. Hernández, M. A. Máñez, E. García-España, C. Soriano, L. Ruiz-Ramírez, B. Verdejo, *Chem. Commun.* **2003**, 3032–3033.
[15] S. Andrés, B. Escuder, A. Doménech, E. García-España, S. V. Luis, V. Marcelino, J. M. Llinares, J. A. Ramírez, C. Soriano, *J. Phys. Org. Chem.* **2001**, *14*, 495–500.
[16] B. Verdejo, S. Blasco, E. García-España, F. Lloret, P. Gaviña, C. Soriano, S. Tatay, H. R. Jiménez, A. Doménech, J. Latorre, *Dalton Trans.* **2007**, 4726–4737.
[17] C. Amatore, J.-M. Saveant, *J. Am. Chem. Soc.* **1981**, *103*, 5021–5023.
[18] a) H. Fujihira, Y. Hirata, K. Suga, *J. Electroanal. Chem.* **1990**, *292*, 199–215; b) M. Shionoya, E. Kimura, Y. Itaka, *J. Am. Chem. Soc.* **1990**, *112*, 9237–9245.
[19] F. Abbà, G. De Santis, L. Fabbrizzi, M. Liccheli, A. M. Manotti Lanfredi, P. Pallavicini, A. Poggi, F. Ugozzoli, *Inorg. Chem.* **1994**, *33*, 1366–1375.
[20] M. R. Rhodes, M. H. Barley, T. J. Meyer, *Inorg. Chem.* **1991**, *30*, 629–635.
[21] J. Hayon, A. Raveh, A. Bettelheim, *J. Electroanal. Chem.* **1993**, *359*, 209–221.
[22] A. Doménech, M. T. Doménech, M. L. Vázquez, *J. Phys. Chem. B* **2006**, *110*, 6027–6039.
[23] A. Doménech, M. T. Doménech, M. L. Vázquez, *J. Solid State Electrochem.* in press.
[24] M. Lovric, F. Scholz, *J. Solid State Electrochem.* **1997**, *1*, 108–113.
[25] M. Lovric, F. Scholz, *J. Solid State Electrochem.* **1999**, *3*, 172–175.
[26] K. B. Oldham, *J. Solid State Electrochem.* **1998**, *2*, 367–377.
[27] U. Schröder, K. B. Oldham, J. C. Myland, P. J. Mahon, F. J. Scholz, *J. Solid State Electrochem.* **2000**, *4*, 314–324.
[28] J. H. Kim, S. V. Lindeman, J. K. Kochi, *J. Am. Chem. Soc.* **2001**, *123*, 4951–4959.
[29] M. C. Jimenez-Molero, C. Dietrich-Buchecker, J.-P. Sauvage, *Chem. Eur. J.* **2002**, *8*, 1456–1466.
[30] E. García-España, M. J. Ballester, F. Lloret, J. M. Moratal, J. Faus, A. Bianchi, *J. Chem. Soc. Dalton Trans.* **1988**, 101–104.
[31] M. Fontanelli, M. Micheloni. *Proceedings of the First Spanish-Italian Congress on Thermodynamics of Metal Complexes*, Peñíscola, Castellón, **1990**. Program for the automatic control of the microburette and the acquisition of the electromotive force readings.
[32] a) G. Gran, *Analyst (London)* **1952**, *77*, 661–671; b) F. J. Rossotti, H. Rossotti, *J. Chem. Educ.* **1965**, *42*, 375–378.
[33] R. L. Vold, J. S. Waugh, M. P. Klein, D. E. Phelps, *J. Chem. Phys.* **1968**, *48*, 3831–3832.
[34] R. C. Engstrom, V. A. Strasser, *Anal. Chem.* **1984**, *56*, 136–141.
[35] K. S. Suslick, S. J. Doktycz, *Adv. Sonochem.* **1990**, *1*, 197–230.
[36] N. A. Madigan, T. J. Murphy, J. M. Fortune, C. R. S. Hagan, L. A. Coury Jr, *Anal. Chem.* **1995**, *67*, 2781–2786.
[37] A. Doménech, H. García, I. Casades, M. Esplá, *J. Phys. Chem. B* **2004**, *108*, 20064–20075.

Received: July 19, 2007
Published Online: November 13, 2007

